Phys. Proc. Ultra-Peripheral Collisions **2**, 021 (2026) 1-8

# Open charm photoproduction in UPCs at the LHC

M. Cacciari[(1,2)], G.M. Innocenti[(3)] and A.M. Staśto[(4),a],
[(1)] *Sorbonne Université, CNRS, Laboratoire de Physique Théorique et Hautes Énergies, LPTHE, F-75005 Paris, France*
[(2)] *Université Paris Cité, LPTHE, F-75006 Paris, France*
[(3)] *Massachusetts Institute of Technology, Cambridge, MA 02139, USA*
[(4)] *Department of Physics, Penn State University, University Park, PA 16802, USA*

We present the calculation for the open charm production in ultraperipheral collisions at the Large Hadron Collider. Predictions for $D^0$ photoproduction using the Generalized-Photon-Nucleus FONLL formalism are presented, extending previously developed framework for electron-proton and electron-nucleus collisions. The calculations are benchmarked against the experimental data for $D^*$ production at HERA collider, with the updated proton distribution function. We present predictions for $D^0$ photoproduction in UPCs, including the photon flux from nucleus, and modifying it by the electromagnetic dissociation probability. The results in bins of transverse momentum and rapidity are compared to the measurements from CMS experiment in UPC lead-lead collisions at $\sqrt{s_{NN}} = 5.36$ TeV at the LHC. We quantify uncertainties due to the renormalization and factorization scale variation, as well as the PDF and fragmentation function uncertainties.

DOI: https://doi.org/10.17161/c4pvdf81
*Keywords:* ultraperipheral collisions, open charm, heavy quarks, nuclear PDFs

## 1 Introduction

Ultraperipheral Collisions (UPCs) are collisions of nuclei, which occur at impact parameter larger than the sum of two radii of these nuclei, for reviews see for example [1,2]. Because of this condition the hadronic component of the interaction is suppressed, and the electromagnetic component dominates in the scattering process. Therefore this is a much cleaner environment than the one in the standard nucleus-nucleus collisions. The photon flux from the nucleus can be computed using equivalent photon approximation [3,4,5,6] and is enhanced by the square of the electric charge of the nucleus. In UPCs one can study photo-nuclear reactions and photon-photon processes. The photo-nuclear reactions can be used to probe the nuclear structure, especially when hard scale is present, which allows for the partonic interpretation and usage of the tools of perturbation theory.

A particularly interesting process is that of the inclusive open charm production in UPCs. This process can be measured as a function of the transverse momentum of the produced charm meson, which in turn gives access to wide range of scales. This inclusive process can be described using the collinear factorization theorem, with universal parton distribution functions. The dominant mechanism for the production of the charm quarks is the photon-gluon fusion, making this process an excellent probe of the gluon distribution in nuclei. It therefore allows for sensitive tests of the QCD evolution of the gluon density[7], and can be useful for quantifying the non-linear effects due to the parton saturation at small $x$.

Recently, the CMS collaboration performed the first measurement [8] of inclusive $D^0$ photoproduction in ultraperipheral PbPb collisions at $\sqrt{s_{\rm NN}} = 5.36$ TeV. The measurement was performed as a function of transverse momentum and rapidity in the ranges $2 < p_T < 12$ GeV and $-2 < y < 2$.

It is therefore essential to provide the accurate calculations for this process, which then can inform about the gluon distribution in the nucleus. We present here the calculation based on the FONLL framework, developed some time ago for photoproduction and hadroproduction of heavy quarks [9,10]. In this framework, the open charm photoproduction was generalized to ultraperipheral nucleus-nucleus collisions. The flux of photons from a nucleus was included, together with the electromagnetic dissociation effect, which describes the survival probability of the nucleus in the presence of the soft electromagnetic interactions. This is necessary to include as the event selection at CMS is the 0nXn, which effectively means there is a requirement on one nucleus to stay intact (0n) and the other to break down (Xn). However, additional soft electromagnetic interactions can lead to the break up of the photon-emitting nucleus, and therefore the correction due to the electromagnetic dissociation needs to be included in the theoretical calculation. In our predictions we also studied nuclear PDF dependence, the sensitivity to the

[a]Speaker, email: ams52@psu.edu

fragmentation and the renormalization and factorization scale dependence. The details of the calculation have been presented in [11].

## 2 Charm photoproduction cross section in FONLL approach

The differential cross section for photoproduction of heavy quarks was obtained from the FONLL framework [9,10] developed for hadroproduction and photoproduction of heavy quarks. It includes resummation of large logarithms of transverse momenta over the mass of the heavy quark, and it smoothly connects the region of small and large transverse momenta of the produced heavy quark. In the low $p_T$ region the fixed order massive approach is valid, and in the large transverse momentum region logarithmically enhanced terms are resummed. The FONLL framework includes terms up to next-to-leading (NLO) order, which corresponds to the terms $\alpha_{\rm em}\alpha_s$ and $\alpha_{\rm em}\alpha_s^2$. These terms are included exactly. In addition in the FONLL approach the resummation of all the logarithmically enhanced terms $\alpha_{\rm em}\alpha_s(\alpha_s \ln(p_T/m))^k$ and $\alpha_{\rm em}\alpha_s^2(\alpha_s \ln(p_T/m))^k$ is performed, which mainly affects the large $p_T$ region. The matched and resummed FONLL cross section is given by [10,12]

$$\text{FONLL} = \text{FO} + (\text{RS} - \text{FOM0}) \times G(m, p_T) \; , \tag{1}$$

where FO denotes fixed order, RS is the resummed result with all the logarithmically enhanced contributions, up to terms suppressed by powers of $m/p_T$ and FOM0 is the massless limit of fixed order FO. The damping function $G(m, p_T)$ is included, which is regular in $p_T$, and approaches unity at large $p_T$. For the photoproduction case, the FONLL formalism includes both the direct and resolved contributions, where the latter require the use of the parton densities in the photon. It is important to note, that formally the division between these two contributions is accurate at lowest order, but not well defined at higher orders in perturbation theory, and is scheme dependent (see discussion in [10]).

The calculation of the charm-production cross section takes as an input parton distribution functions in the target nucleon or nucleus. For the nuclear parton distribution functions, we have selected EPPS21 [13] and nNNPDF3.0 [14] parametrizations. For calculations without the nuclear effects we have used CT18ANLO [15] proton PDF (which was used as a baseline PDF for EPPS21 analysis).

For the resolved contribution photon PDF needs to be used, we have used standard choices available in the FONLL code, AFG [16] and GRV [17] PDF distributions.

Another ingredient in the calculation is the fragmentation function which describes the transition from the quark to the hadron. This is a non-perturbative function which needs to be parametrized, with parameters adjusted to fit the experimental data. In the present analysis we have used two parametrizations : the Peterson-Schlatter-Schmitt-Zerwas (PSSZ) [18] and Braaten–Cheung–Fleming–Yuan (BCFY) [19] fragmentation functions.

## 3 Photon flux and electromagnetic dissociation

### *3.1 Photon flux from nucleus*

For the case of the UPCs, one needs to fold into the calculation the photon flux from the nucleus. We used the analytic expression, for example presented in[1], which was obtained in the pointlike approximation:

$$f_{\gamma/A}(z) = \int d^2\mathbf{b}\, \tilde{f}_{\gamma/A}(z, \mathbf{b})\, \theta(|\mathbf{b}| - b_{\rm min}) = \frac{2Z^2\alpha_{em}}{\pi z} \left[ \eta K_0(\eta) K_1(\eta) - \frac{\eta^2}{2}(K_1(\eta)^2 - K_0(\eta)^2) \right] , \tag{2}$$

with the dimensionless variable $\eta$ defined as

$$\eta = \frac{z\, m_p\, b_{\rm min}}{\hbar c} \; . \tag{3}$$

In Eq. (2) $\tilde{f}_{\gamma/A}(z, \mathbf{b})$ is the photon flux of the nucleus evaluated at the transverse distance $\mathbf{r} = \mathbf{b}$ where $\mathbf{b}$ is vector connecting the centers of the two nuclei in the transverse plane of the collision. This is justified in the pointlike approximation of the nucleus. The pointlike flux is expressed in terms of modified Bessel functions $K_0$ and $K_1$. Note the appearance of the $Z^2$ factor, where $Z$ is the atomic number ($Z = 82$ for lead). This is responsible for the enhancement of the photon flux from a large nucleus. In the definition of the dimensionless variable $\eta$, there is $z$ which is the fraction of the energy of the nucleus carried by the photon, $m_p$ is the proton mass and $b_{\rm min}$ distance between the nuclei. Following [20,21,22] we take the impact parameter $b_{\rm min} = 2R = 14.2$ fm, with $R = 7.1$ fm being the nuclear hard-sphere radius, to account for the finite size of the colliding nuclei.

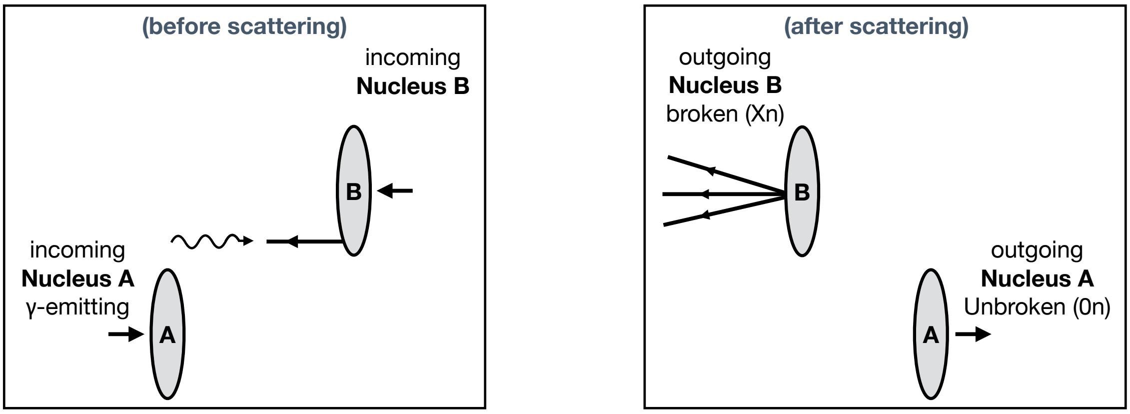


Figure 1 – Sketch of an ultraperipheral heavy-ion collision before (left) and after (right) the scattering. The photon emitting nucleus is coming from the left and the parton emitting one from the right. The experimental selection 0nXn, means that there is requirement of the unbroken nucleus on one side (0n) and broken nucleus on the other side (Xn).

### *3.2 Modeling of the no-breakup probability in UPCs*

The UPC events for the photonuclear case, where one of the nuclei emits a photon and the other is broken, are selected by the 0nXn requirement. This is illustrated in Fig. 1. The 0n selection means that there are no neutrons in the zero-degree calorimeter (ZDC) in one direction. The Xn selection means, there is at least one neutron in the opposite ZDC, thus signaling a nuclear break-up. Therefore the unbroken nucleus is the one likely emitting a photon, and the broken nucleus is the one that emitted a parton. This selection is accompanied by the requirement of the rapidity gap in the 0n direction. Such setup allows for the selection of the photo-nuclear events and suppression of the hadronic events, which mainly lead to configurations XnXn as well as the two-photon processes mainly dominating the 0n0n.

This selection means however that the experimental measurement is not entirely inclusive, in contrast to the theoretical calculation which is defined and set up for the inclusive photoproduction of charm meson. Additional soft electromagnetic interactions between two colliding nuclei can lead to the break-up of the photon-emitting nucleus. This is referred to as the electromagnetic dissociation or EMD. Therefore one has to include the possibility that the photonuclear event, in which the nucleus is initially left unbroken, is rejected by the selection of 0nXn, due to the subsequent soft electromagnetic interaction which leads to its breakup.

The no-breakup probability therefore has to be included in the theoretical calculation. This is done under the assumption that the soft electromagnetic interactions leading to the break-up factorize from the rest of the interactions. For the calculation we used an effective photon flux, with the no-breakup probability folded in, as presented in[22,23].

The size of the electromagnetic dissociation factor is illustrated in Fig. 2, where in the left panel we show the ratio of the effective photon flux with EMD to the standard photon flux from the nucleus given by Eq. (2). This quantity represents the no-breakup probability as a function of the photon energy fraction $z$. We observe that the ratio between the two fluxes decreases significantly, from about 0.9 at low $z$, to 0.2 with increasing photon energy. This is due to the fact that the probability of the electromagnetic dissociation is enhanced for small impact parameters, which also correspond to the region of the largest energies of the photons.

The effective photon flux with EMD is then used to compute the cross section for the $D^0$ production as a function of transverse momentum and rapidity. This is shown in the right panel of Fig. 2, where we present the ratio of the calculated double-differential cross section from G$\gamma$A-FONLL with EMD effect to the one obtained without this correction. The calculation uses EPPS21 nuclear PDFs, the BCFY fragmentation function, and a charm-quark mass of $m_c = 1.3$ GeV. The resulting no-break-up probability, which was used to reweight the $D^0$ double-differential cross sections in UPCs, ranges from 0.83 to 0.68 for $D^0$ mesons with $0 < p_T < 1$ GeV and from 0.71 to 0.45 for those with $11 < p_T < 12$ GeV.

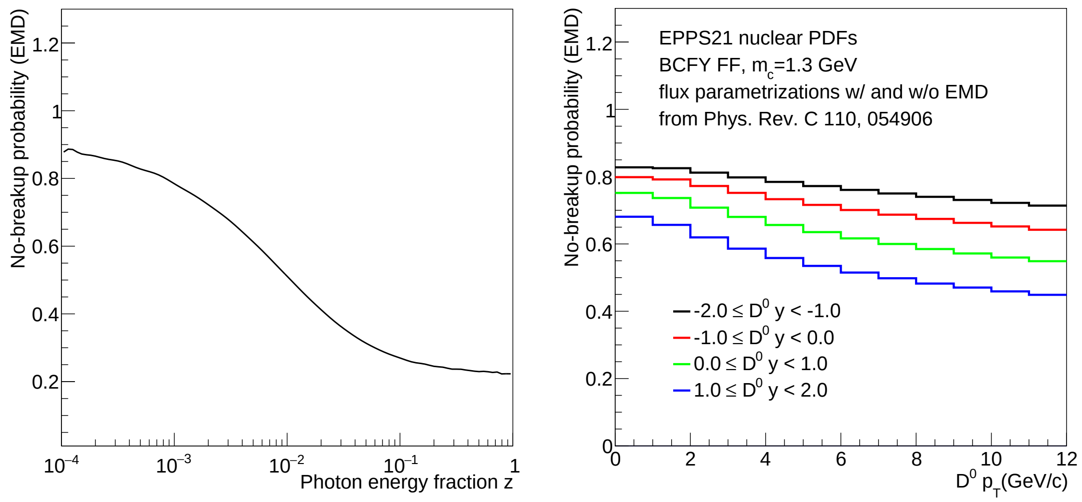


Figure 2 – (Left) No-breakup probability (EMD) as a function of the photon-energy fraction $z$. (Right) No-breakup probability (EMD) as a function of the $D^0$ $p_T$, in different intervals of the $D^0$ rapidity $y$. The interpolated Chebyshev parametrizations of the photon fluxes used to compute these ratios are taken from [22]. Figure from [11].

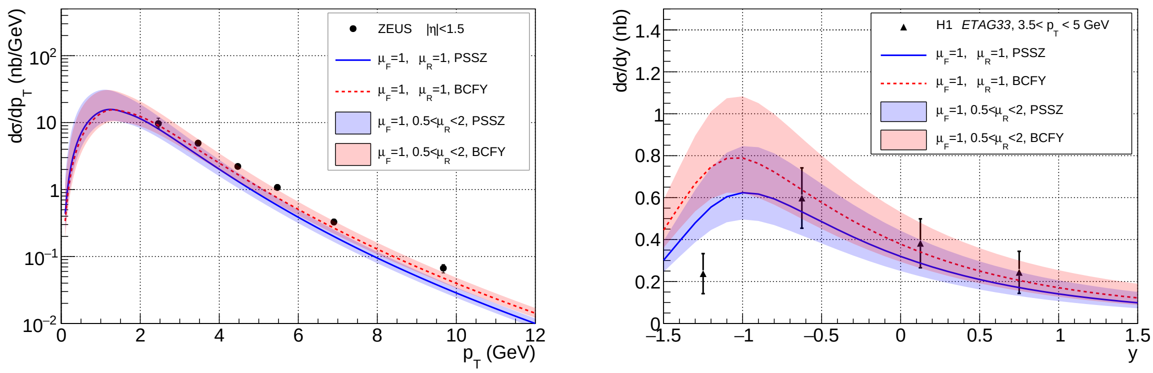


Figure 3 – Left: transverse momentum distribution for the $D^*$ photoproduction compared with the ZEUS data [24]. Right: rapidity distribution for the $D^*$ production compared to the H1 data [25]. Blue curve: calculation using the PSSZ [18] fragmentation function, red-dashed curve: calculation using BCFY fragmentation function [19]. Bands indicate the renormalization scale variation $0.5 < \mu_R < 2$. Figure from [11].

## 4 Comparison with HERA data

The FONLL formalism was used to perform calculations and comparisons with the HERA data on $D^*$ production in the past [12]. We have revisited and updated these calculations with newer PDFs and tested the sensitivity to the variation of the fragmentation functions. In Fig.3 (left) we show the example of the $p_T$ distribution for selection of the ZEUS data [24], and rapidity distributions for the selection of data from H1 [25] (right plot). In both cases CT18ANLO parton distribution was used.

Solid blue curves are for the calculation with the PSSZ[18] fragmentation function and red-dashed curve is for the case with BCFY[19] fragmentation function, for central choice of the renormalization and factorization scale $\mu_R = \mu_F = 1$. The bands indicate the renormalization scale variation $0.5 < \mu_R < 2$, with factorization scale fixed $\mu_F = 1$. The variation of the latter is negligible with respect to the renormalizations scale variation, except for the lowest values of $p_T$ (see also [12]). We see that the agreement with the data is fair, though the calculations seem a little softer in the $p_T$ dependence than the data. Overall the BCFY fragmentation function is giving a better description. The rapidity distribution is described fairly well, given the sizeable errors of the experimental data.

Overall, we find a reasonable agreement of the FONLL calculation with the experimental data from HERA, which provides an important benchmark for the predictions in UPC collisions.

## 5 Predictions for $D^0$ production in UPC and comparison with CMS data

In Fig. 4 we show a double differential cross section for the $D^0$ photoproduction in PbPb UPCs at LHC in the CMS binning: three bins in $p_T$ (2-5), (5-8), (8-12) GeV. The rapidity range is (-2,2) (4 bins) for two highest $p_T$ bins and (-1,1) for the lowest $p_T$ bin (1 bin in rapidity). The calculations were performed using EPPS21 (left column) and nNNPDF3.0 (right column) nuclear PDFs and with BCFY fragmentation function. For the EPPS21 calculation two charm mass choices were selected $m_c = 1.3$ (blue bands) and $m_c = 1.5$ GeV (magenta bands), for nNNPDF3.0 calculation only $m_c = 1.5$ GeV mass is shown. The thinner bands indicate the PDF uncertainty, while the broader bands correspond to the renormalization and factorization scale variation $1/2\mu_0 \leq \mu_R, \mu_F \leq 2\mu_0$ with $1/2 \leq \mu_R/\mu_F$, and scale $\mu_0 = \sqrt{p_T^2 + m_c^2}$. The black points are CMS data [26]. We observe a fairly good agreement between the experimental data and the calculation. In more detail the calculation tends to be slightly on the higher side of the data for very low $p_T$ and a bit on the lower side for high $p_T$, but within the uncertainties. The calculations with the higher value of the charm mass seem to describe the data better. One has to caution however, since the calculation is sensitive to the choices of the fragmentation function parameters and the parton distribution functions.

In Fig. 5 we show the same data compared to the calculation using the CT18ANLO parton distribution function, which is the proton baseline for the EPPS21. Therefore the calculation does not include a nuclear shadowing. We observe that the calculation is markedly higher than the data for lowest bin in transverse momenta, indicating the need for inclusion of the nuclear effects in the calculation.

It is instructive to perform an estimate of the $x, Q^2$ range at which gluon density is probed through open-charm observables in ultra-peripheral collisions. To this aim one can approximate the transverse momentum scale $Q^2$ with the squared transverse mass of the charm quark $m_T^2 = p_T^2 + m_c^2$ and the target's longitudinal momentum carried by the parton as $x \approx m_T/\sqrt{s_{\rm NN}}\, e^{-y_c}$, where $m_c$ is the charm quark mass, $\sqrt{s_{\rm NN}}$ is the center-of-mass energy of the nucleon-nucleon system, and $p_T$ is the transverse momentum of the charm quark.

The predicted $(x, Q^2)$ region probed by open-charm measurements in UPCs at $\sqrt{s_{\rm NN}} = 5.36$ TeV obtained using this estimate is shown in Fig. 6. The charm-quark transverse momentum is selected to be in the range $0 < p_{T,c} < 12$ GeV and rapidity $-2.4 < y_c < 2.4$. This kinematic region, enables the exploration of $x$ values from approximately 0.01 down to below $10^{-4}$, and $Q^2$ values ranging from $m_c^2$ up to around $\sim 100\,\mathrm{GeV}^2$. We note however that this is rather crude an estimate, as it does not take into account fragmentation and neglects the kinematics of the other charm-quark which was pair-produced in the photon-gluon fusion.

## 6 Conclusions

We have presented a calculation of the open charm production in UPCs using the G$\gamma$A-FONLL formalism. This formalism is based on the FONLL framework and extended to include the photon flux from the nucleus and accounting for the electromagnetic dissociation factor. This was performed in order to be able to compare the theoretical calculations for the inclusive production with the experimental data based on the 0nXn selection. The calculation is in good agreement with the experimental data from CMS in the measured kinematical range of rapidity and transverse momenta. The calculation using nuclear PDFs agrees with the experimental data, whereas the calculation using proton PDFs overestimates the data at low values of the transverse momentum, indicating the need for the nuclear effects. We have also studied the sensitivity of the calculation to the renormalization and factorization scale dependence, the fragmentation function, parton distribution choices and the variation with the charm quark mass.

### Acknowledgments

GMI is supported by the U.S. Department of Energy grant No. DOE-SC0011088. AMS is supported by the U.S. Department of Energy grant No. DE-SC-0002145 and within the framework of the of the Saturated Glue (SURGE) Topical Theory Collaboration.

### References

1. Carlos A. Bertulani and Gerhard Baur. Electromagnetic Processes in Relativistic Heavy Ion Collisions. *Phys. Rept.*, 163:299, 1988.
2. A. J. Baltz. The Physics of Ultraperipheral Collisions at the LHC. *Phys. Rept.*, 458:1–171, 2008.

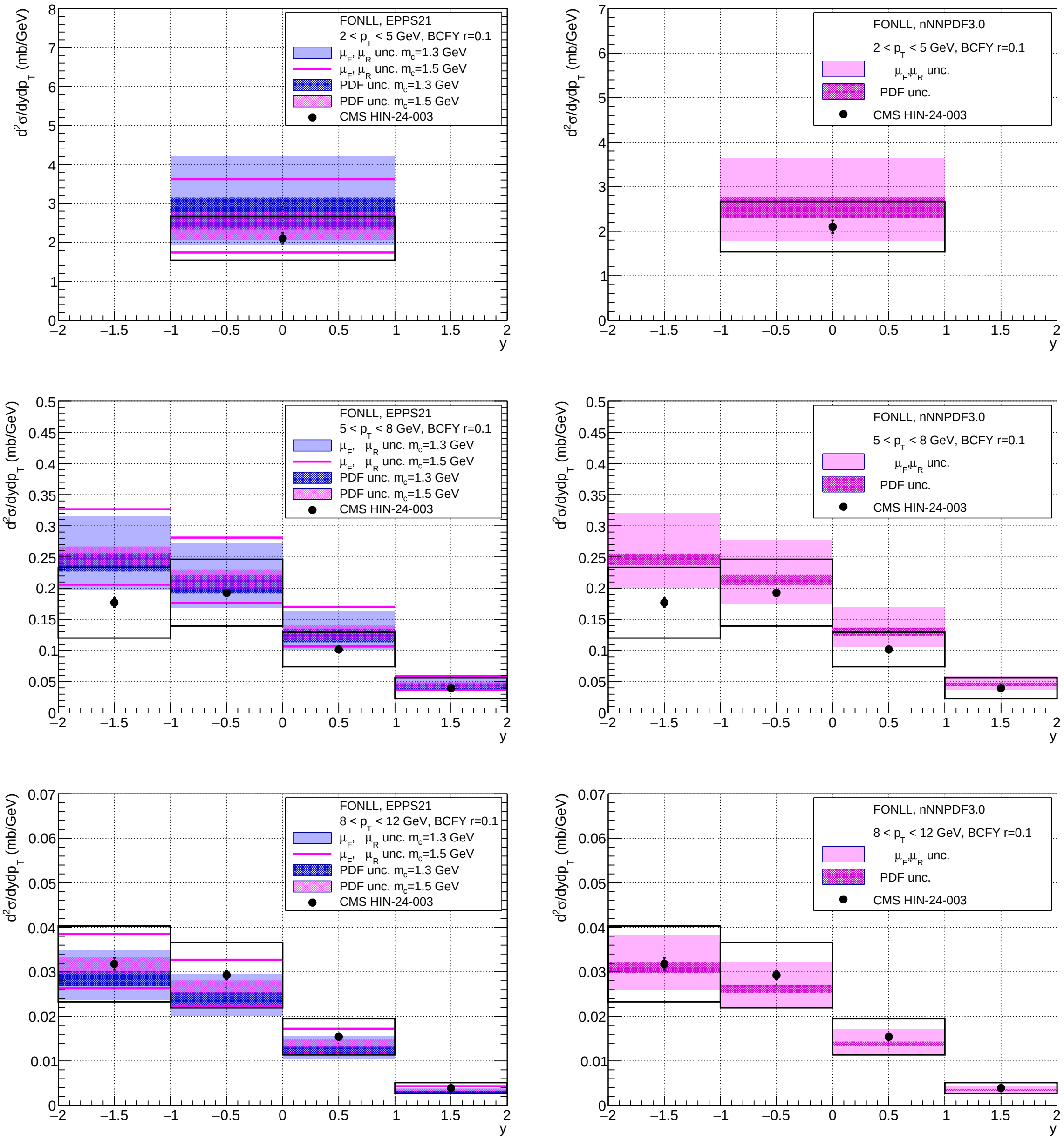


Figure 4 – Left column: Rapidity distribution for the $D^0$ photoproduction in UPC PbPb collisions at $\sqrt{s_{\mathrm{NN}}} = 5.36$ TeV with EPPS21 nuclear PDF in $p_T$ bins $(2-5), (5-8), (8-12)$ GeV. Light blue band: FONLL calculation with factorization and renormalization scale variation for $m_c = 1.3\,\mathrm{GeV}$, magenta lines band: FONLL calculation with factorization and renormalization scale variation and $m_c = 1.5\,\mathrm{GeV}$, dark blue band: FONLL EPPS21 [13] PDF uncertainty, $m_c = 1.3\,\mathrm{GeV}$. Magenta band: FONLL EPPS21 [13] PDF uncertainty, $m_c = 1.5\,\mathrm{GeV}$. BCFY fragmentation function [19,27] with parameter $r = 0.1$. Data are from CMS [26]. Right column: the calculation is performed with nNNPDF3.0 nuclear prton distribution, charm mass set to $m_c = 1.5$GeV. Figure from [11].

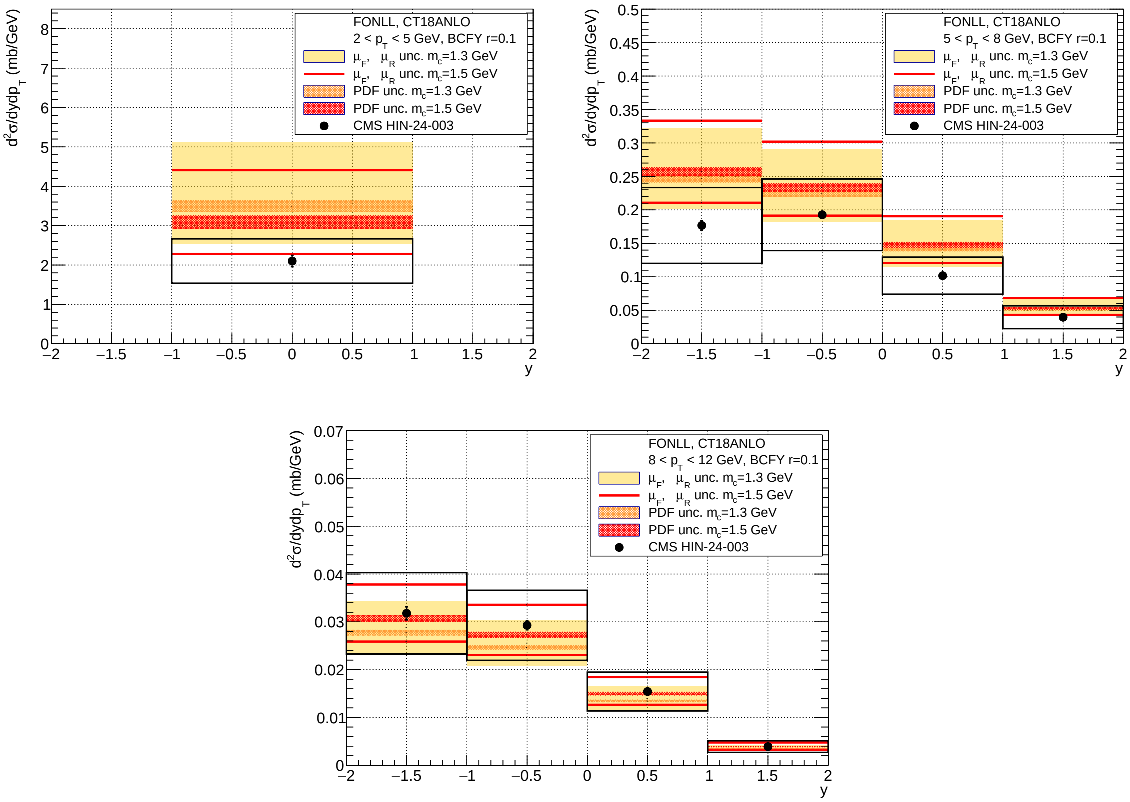


Figure 5 – Rapidity distribution for the $D^0$ photoproduction in UPC PbPb collisions at $\sqrt{s_{\rm NN}} = 5.36$ TeV with CT18ANLO proton PDF in $p_T$ bins $(2-5), (5-8), (8-12)$ GeV. Yellow band: FONLL calculation with factorization and renormalization scale variation for $m_c = 1.3\,$GeV, red lines band: FONLL calculation with factorization and renormalization scale variation and $m_c = 1.5\,$GeV, orange band: FONLL CT18ANLO PDF uncertainty, $m_c = 1.3\,$GeV. Red band: FONLL CT18ANLO [13] PDF uncertainty, $m_c = 1.5\,$GeV. BCFY fragmentation function [19,27] with parameter $r = 0.1$. Data are from CMS [26]. Figure from [11].

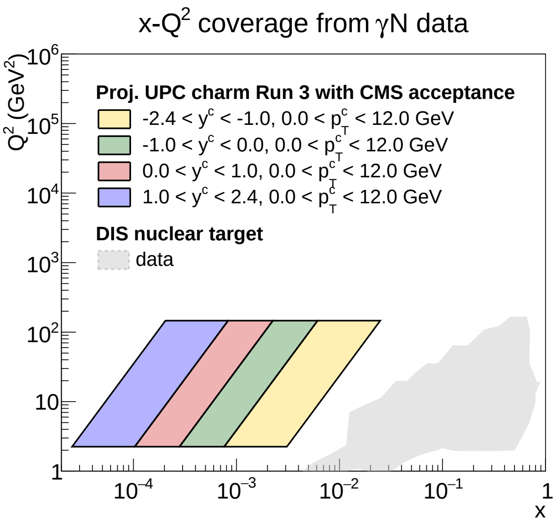


Figure 6 – $x$ and $Q^2$ coverage charm production in UPCs collisions. In grey, the existing coverage from fixed-target deep-inelastic photonuclear measurements is presented [28]. Figure from [11].

3. E. Fermi. On the Theory of the impact between atoms and electrically charged particles. *Z. Phys.*, 29:315–327, 1924.
4. Enrico Fermi. On the theory of collisions between atoms and electrically charged particles. *Nuovo Cim.*, 2:143–158, 1925.
5. E. J. Williams. Nature of the high-energy particles of penetrating radiation and status of ionization and radiation formulae. *Phys. Rev.*, 45:729–730, 1934.
6. C. F. von Weizsacker. Radiation emitted in collisions of very fast electrons. *Z. Phys.*, 88:612–625, 1934.
7. Mark Strikman, Ramona Vogt, and Sebastian N. White. Probing small x parton densities in ultraperipheral AA and pA collisions at the LHC. *Phys. Rev. Lett.*, 96:082001, 2006.
8. Vladimir Chekhovsky et al. Measurement of $D^0$ meson photoproduction in ultraperipheral heavy ion collisions. 9 2025.
9. Matteo Cacciari, Mario Greco, and Paolo Nason. The $p_T$ spectrum in heavy-flavour hadroproduction. *JHEP*, 05:007, 1998.
10. Matteo Cacciari, Stefano Frixione, and Paolo Nason. The p(T) spectrum in heavy flavor photoproduction. *JHEP*, 03:006, 2001.
11. Matteo Cacciari, Gian Michele Innocenti, and Anna M. Staśto. Inclusive open charm photoproduction in ultraperipheral collisions at the LHC with in the generalized photon-nucleus fixed-order next-to-leading logarithm framework. *Phys. Rev. D*, 112(9):094029, 2025.
12. Stefano Frixione and Paolo Nason. Phenomenological study of charm photoproduction at HERA. *JHEP*, 03:053, 2002.
13. Kari J. Eskola, Petja Paakkinen, Hannu Paukkunen, and Carlos A. Salgado. EPPS21: a global QCD analysis of nuclear PDFs. *Eur. Phys. J. C*, 82(5):413, 2022.
14. R. Abdul Khalek et al. Science Requirements and Detector Concepts for the Electron-Ion Collider: EIC Yellow Report. *Nucl. Phys. A*, 1026:122447, 2022.
15. Tie-Jiun Hou et al. New CTEQ global analysis of quantum chromodynamics with high-precision data from the LHC. *Phys. Rev. D*, 103(1):014013, 2021.
16. P. Aurenche, J. P. Guillet, and M. Fontannaz. Parton distributions in the photon. *Z. Phys. C*, 64:621–630, 1994.
17. E. Reya M. Glück and A. Vogt. Photonic parton distributions. Phys. Rev. D 46, 1973, 09 1992.
18. C. Peterson, D. Schlatter, I. Schmitt, and Peter M. Zerwas. Scaling Violations in Inclusive e+ e- Annihilation Spectra. *Phys. Rev. D*, 27:105, 1983.
19. Eric Braaten, King-man Cheung, Sean Fleming, and Tzu Chiang Yuan. Perturbative QCD fragmentation functions as a model for heavy quark fragmentation. *Phys. Rev. D*, 51:4819–4829, 1995.
20. J. Nystrand. Electromagnetic interactions in nucleus-nucleus and proton-proton collisions. *Nucl. Phys. A*, 752:470–479, 2005.
21. V. Guzey and M. Klasen. Inclusive dijet photoproduction in ultraperipheral heavy ion collisions at the CERN Large Hadron Collider in next-to-leading order QCD. *Phys. Rev. C*, 99(6):065202, 2019.
22. Kari J. Eskola, Vadim Guzey, Ilkka Helenius, Petja Paakkinen, and Hannu Paukkunen. Spatial resolution of dijet photoproduction in near-encounter ultraperipheral nuclear collisions. *Phys. Rev. C*, 110(5):054906, 2024.
23. Petja Paakkinen, Kari J. Eskola, Vadim Guzey, Ilkka Helenius, and Hannu Paukkunen. Collision geometry in UPC dijet production. *Phys. Proc. UPC*, 1:16, 2024.
24. J. Breitweg et al. Measurement of inclusive D*+- and associated dijet cross-sections in photoproduction at HERA. *Eur. Phys. J. C*, 6:67–83, 1999.
25. C. Adloff et al. Measurement of D* meson cross-sections at HERA and determination of the gluon density in the proton using NLO QCD. *Nucl. Phys. B*, 545:21–44, 1999.
26. Constraining nuclear parton dynamics with the first measurement of D0-photoproduction in ultra-peripheral heavy-ion collisions at the LHC. 2024. CMS-PAS-HIN-24-003.
27. Matteo Cacciari and Paolo Nason. Charm cross-sections for the Tevatron Run II. *JHEP*, 09:006, 2003.
28. Rabah Abdul Khalek, Jacob J. Ethier, and Juan Rojo. Nuclear parton distributions from lepton-nucleus scattering and the impact of an electron-ion collider. *Eur. Phys. J. C*, 79(6):471, 2019.